Research article **Open Access**

Binjie Zheng, Yuanfu Chen*, Pingjian Li, Zegao Wang, Bingqiang Cao, Fei Qi, Jinbo Liu, Zhiwen Qiu and Wanli Zhang

Ultrafast ammonia-driven, microwave-assisted synthesis of nitrogen-doped graphene quantum dots and their optical properties

DOI 10.1515/nanoph-2016-0102
Received January 7, 2016; revised February 21, 2016; accepted February 22, 2016

Abstract: For the first time, a facile, ultrafast, ammonia-driven microwave-assisted synthesis of high-quality nitrogen-doped graphene quantum dots (NGQDs) at room temperature and atmospheric pressure is presented. This one-step method is very cheap, environment friendly, and suitable for large-scale production. The as-synthesized NGQDs consisting of one to three graphene monolayers exhibit highly crystalline quality with an average size of 5.3 nm. A new fluorescence (FL) emission peak at 390 nm is observed, which might be attributed to the doped nitrogen atoms into the GQDs. An interesting red-shift is observed by comparing the FL excitation spectra to the UV-visible absorption spectra. Based on the optical properties, the detailed Jablonski diagram representing the energy level structure of NGQDs is derived.

Keywords: nitrogen-doped; graphene quantum dots; ultrafast synthesis; fluorescence nanophotonics.

***Corresponding author: Yuanfu Chen,** State Key Laboratory of Electronic Thin Films and Integrated Devices, University of Electronic Science and Technology of China, Chengdu 610054, P.R. China, e-mail: yfchen@uestc.edu
Binjie Zheng, Pingjian Li, Fei Qi, Jinbo Liu and Wanli Zhang: State Key Laboratory of Electronic Thin Films and Integrated Devices, University of Electronic Science and Technology of China, Chengdu 610054, P.R. China
Zegao Wang: Interdisciplinary Nanoscience Center, Aarhus University (iNANO), DK-8000 Aarhus C, Denmark
Bingqiang Cao and Zhiwen Qiu: School of Materials Science and Engineering, University of Jinan, No. 336, West Road of Nan Xinzhuang, Jinan 250022, Shandong, P.R. China

Edited by Volker Sorger

1 Introduction

As a novel type of metal-free fluorescent materials, graphene quantum dots (GQDs) have gained remarkable interest, because their unique broadband and tunable photoemission properties are controlled by the quantum confinement effect and edge states [1–3]. In addition, GQDs have other advantages, such as good water solubility, low toxicity, and biocompatibility. These enable GQDs to be used in photovoltaic devices [4], bioimaging [5], biosensing [6], and environmental monitoring [7]. The doping of nitrogen into GQDs (NGQDs) gives rise to much more attractive properties, such as electrocatalytic activity [8, 9], photocatalytic activity [10, 11], biocompatibility [12], selective detection [13], and broad tunable luminescence [14].

In general, there are two main methods to synthesize NGQDs, i.e. multistep method and one-step method. Multistep methods usually require the synthesis of graphene oxide (GO), reduced GO (rGO), or GQDs first, and then nitrogen doping is performed by electrochemical generation [8], hydrothermal methods [12, 13, 15–18], or high-temperature treatment [11]. Some of these methods need further chemical tailoring to cut nitrogen-doped graphene into NGQDs [11, 18]. In addition, multistep methods include organic synthesis [9], arc discharge [19], and steaming procedure [20]. Obviously, multistep methods are a little complicated.

To overcome such issue, several one-step methods have been developed. For example, NGQDs have been synthesized using glycine [21], glucose [14], or citric acid [22–27] as carbon source or using ammonia [14, 22, 23], dicyandiamide [24, 25], tris(hydroxymethyl) aminomethane [26], 3,4-dihydroxy-L-phenylalanine [27], or glycine [21] as nitrogen source through hydrothermal reaction [14, 21–25] or high-temperature treatment [26, 27]. Such one-step methods usually require high temperature and/or high pressure. Generally, the reaction temperature

should be higher than the normal glycosidation temperature (160–180°C) leading to aromatization and carbonization [28]. This means that the glucose aqueous solution is relatively stable and difficult to be transformed to GQDs at room temperature and atmospheric pressure.

Recently, there are two important progresses to synthesize GQDs or carbon quantum dots using glucose solution source: when the ammonia as catalyst was added into glucose solution, the GQDs can be indeed formed even at room temperature and atmospheric pressure, although it will take about 8 months to complete the reaction [29]; microwave can enhance the carbonization process and thus accelerate the reaction rate in the presence of surface passivation reagent [30] or metal salt catalyst [31]. However, until now, to the best of our knowledge, there are not any reports on the ultrafast synthesis of high-quality NGQDs at room temperature and atmospheric pressure.

Herein, for the first time, by combining both advantages of the catalytic effect of ammonia and the rapid reaction of microwave, we present a facile method to ultrafast synthesize high-quality NGQDs even at room temperature and atmospheric pressure using glucose and ammonia solution in a commercial microwave oven. Glucose acts as a carbon source, ammonia can not only act as a catalyst of dehydration between glucose molecules and the aqueous solution but also act as nitrogen doping source, and microwave can significantly accelerate the reaction rate and guarantee the ultrafast synthesis of NGQDs within 1 min. This one-step, ammonia-driven microwave-assisted synthesis is very cheap, environment friendly, and suitable for large-scale production. The morphology, crystalline structure, and optical properties of the as-synthesized NGQDs have been systematically investigated.

2 Results and discussion

The NGQDs in this study were prepared using glucose and ammonia solution in a commercial microwave oven at room temperature and atmospheric pressure. It is noted that both ammonia and microwave are extremely crucial to ultrafast form NGQDs. However, as reported previously [29], without microwave irradiation, it will take several months to produce NGQDs using glucose and ammonia, which suggests that microwave can provide rapid heating and accelerate the glucose polymerization and carbonization to form NGQDs. On the contrary, our control experiment demonstrates that, when the glucose solution without ammonia was irradiated by microwave, no GQDs were formed, which suggests that the ammonia can not only act as the nitrogen doping source but also act as a catalyst of dehydration between glucose molecules and the aqueous solution to form NGQDs. Therefore, the reaction is ammonia driven and microwave assisted. When both factors (ammonia and microwave) are simultaneously satisfied, the reaction can be effectively driven and significantly accelerated even at room temperature and atmospheric pressure. The reaction is ultrafast, and it will take <1 min to form monodispersed NGQDs. As mentioned above, the formation mechanism of NGQDs can be schematically shown in Figure 1.

The morphology and distribution of NGQDs were characterized by transmission electron microscopy (TEM). As shown in Figure 2A, NGQDs show spherical shape with monodispersed distribution, which can be fitted by a Gaussian curve (Figure 2B). The average size of NGQDs is 5.3 nm with a full-width-at-half-maximum (FWHM) of 1.5 nm. The X-ray diffraction (XRD) pattern of NGQDs is shown in Figure 2C. The diffraction peak at 2θ=22.4° corresponds to a d spacing of 0.40 nm along the (002) direction, which is larger than that of graphite (0.334 nm). The larger d_{002} spacing of our NGQDs can be attributed to the presence of the functional groups and nitrogen doping atoms enlarging the basal plane spacing, which is similar to those of NGQDs prepared by other methods [26, 29, 32]. The atomic force microscopy (AFM) image (Figure 2D) indicates that the typical topographic heights of NGQDs

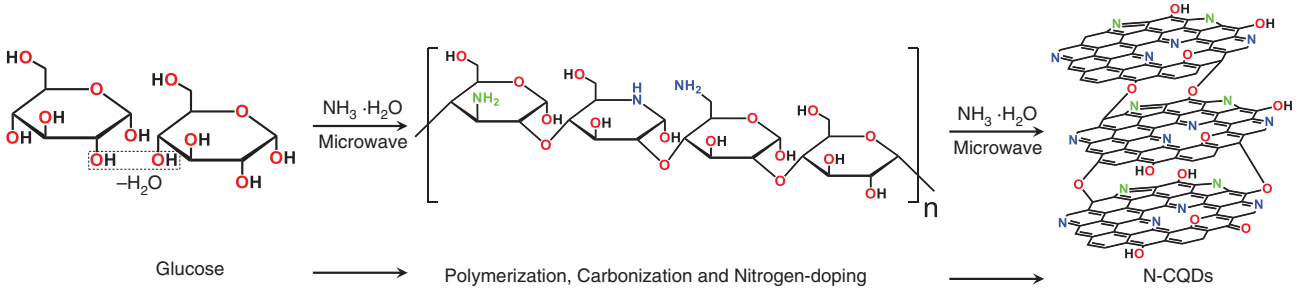

Figure 1: Schematic growth model for NGQDs.

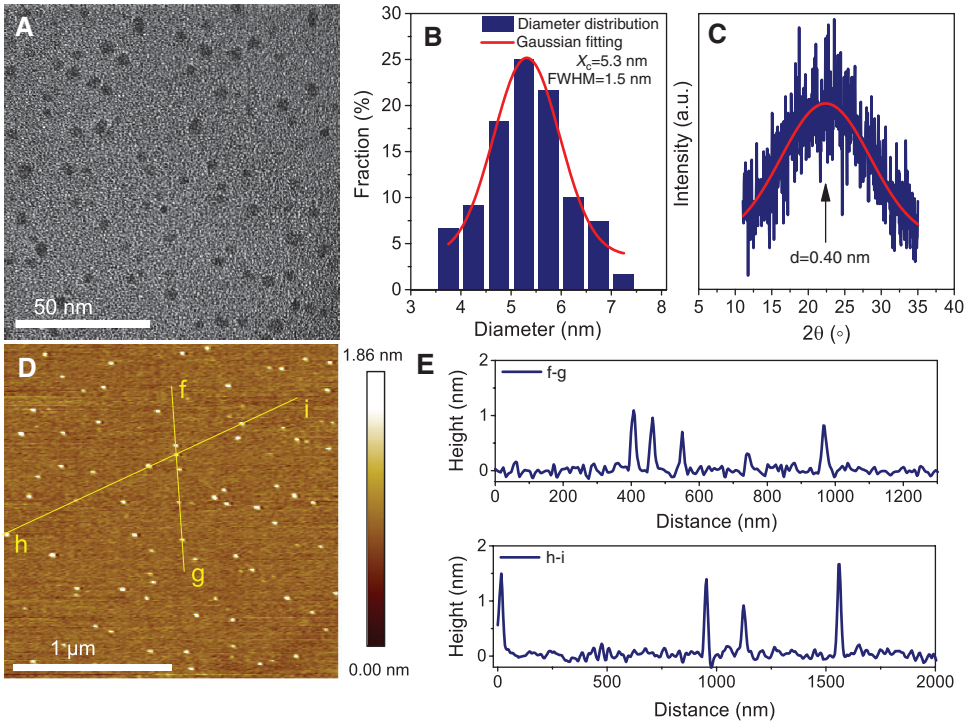

Figure 2: (A) TEM image of NGQDs assembled on a Cu grid coated with an ultrathin amorphous carbon film. (B) Diameter distribution of NGQDs. The red line is the Gaussian fitting curve. The average size (X_c) of NGQDs is 5.3 nm with an FWHM of 1.5 nm. (C) XRD pattern of NGQDs. (D) AFM image of NGQDs on a mica substrate. (E) Height profile along the lines marked in (D).

range from 0.5 to 1.5 nm (Figure 2E), suggesting that most NGQDs consist of one to three graphene monolayers.

To further confirm whether the quantum dots are carbon dots or graphene dots, high-resolution TEM (HRTEM) images of NGQDs with different lattice planes were performed. As shown in Figure 3, one can find that NGQDs exhibit high crystalline quality as revealed by the presence of the lattice fringes. The distances between the lattice fringes are 0.346 nm (Figure 3A), 0.214 nm (Figure 3B), and 0.246 nm (Figure 3C), which correspond to the basal plane spacing (d_{002}=0.334), in-plane lattice spacing (d_{100}=0.213), and in-plane lattice constant (d=0.246) of graphite, respectively [14]. It is worth noting that the basal plane distance (0.346 nm) is slightly larger than that of bulk graphite (0.334 nm) due to the presence of the functional groups and nitrogen doping atoms that enlarge the basal plane spacing of NGQDs. The fast Fourier transform (FFT) image of a selected area (red square) is shown in the inset of Figure 3D, which reveals a hexagonal structure, further confirming the graphene structure. Therefore, it is concluded that our quantum dots are not carbon quantum dots but GQDs.

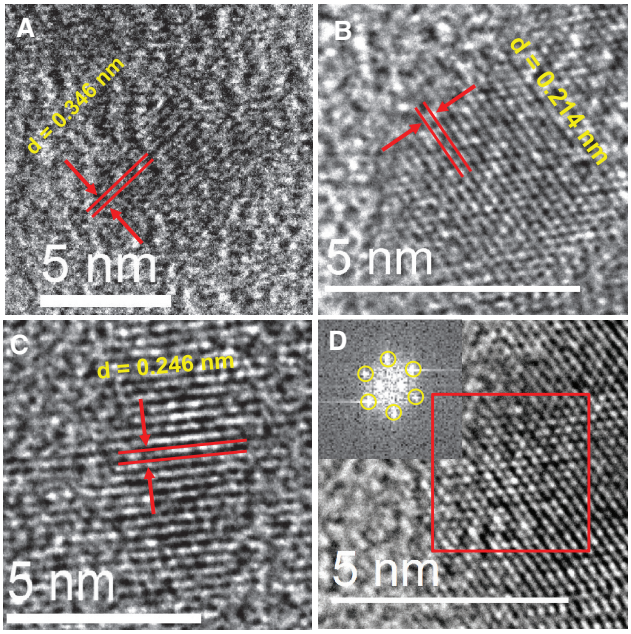

Figure 3: (A–C) HRTEM images of NGQDs, in which three lattice fringes of 0.346, 0.214, and 0.246 nm are observed. (D) FFT image (inset) of a selected area (red square), in which the hexagonal crystal structure is revealed with a lattice parameter of 0.214 nm.

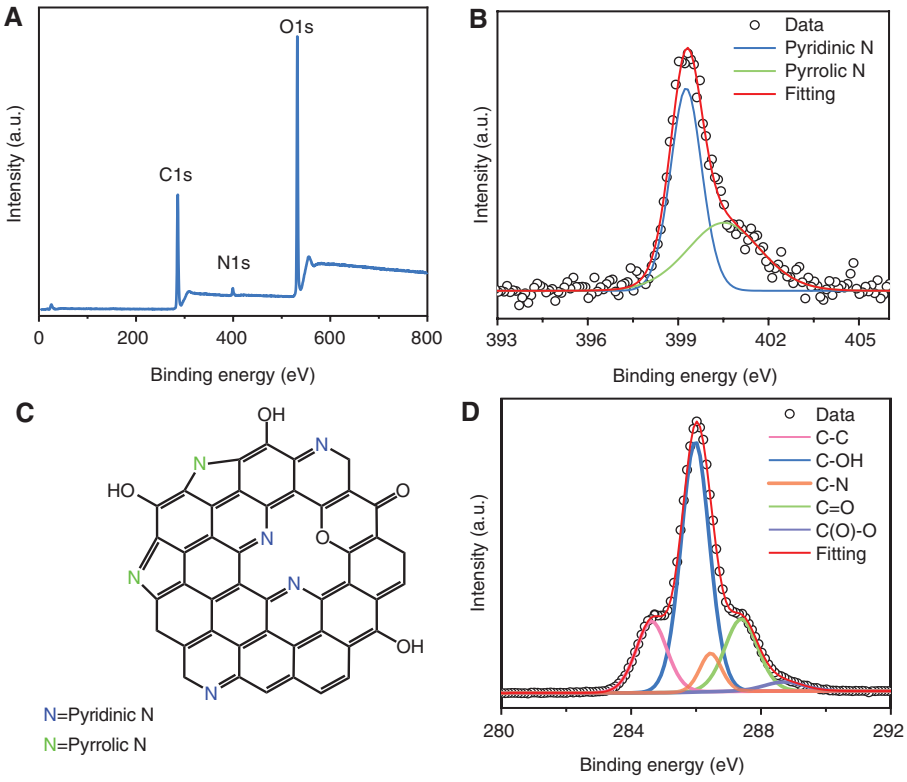

Figure 4: (A) Full-scan XPS spectrum of NGQDs. (B) High-resolution N 1s spectra of NGQDs. (C) Schematic of pyridinic (blue) and pyrrolic (green) N atoms. (D) High-resolution C 1s spectra of NGQDs.

The electronic structure and doping configuration of NGQDs was further characterized by the X-ray photoelectron spectroscopy (XPS) measurements. The full-scan XPS spectrum of NGQDs is shown in Figure 4A. Clearly, three peaks located at approximately 286.1, 399.6, and 532.1 eV correspond to C 1s, N 1s, and O 1s, respectively. The calculated O/C atomic ratio is 67.9%, demonstrating that NGQDs have a relatively higher oxidation level, which is similar to a previous report [15]. The nitrogen doping content is as large as 4.1%, which is comparable to that of NGQDs reported previously [8]. The high-resolution N 1s spectrum of NGQDs (Figure 4B) reveals the presence of both pyridine (399.3 eV) and pyrrolic (400.5 eV) N atoms. Figure 4C shows these two configurations of doped N schematically, which is similar to those of nitrogen-doped film [33] and NGQDs [13]. The result of deconvolution treatment for the high-resolution C 1s spectrum of NGQDs (Figure 4D) reveals five peaks at 284.6 (C-C, sp^2 bonded carbon), 286.0 (C-OH, hydroxyl), 286.5 (C-N), 287.4 (C=O, carbonyl), and 288.7 eV (C(O)-O, carboxyl) [12], which is consistent with the corresponding Fourier transform infrared (FTIR) spectrum (Figure S2). It is noted that the presence of functional groups such as hydroxyl, carbonyl, and carboxyl make NGQDs water-soluble and very stable. The NGQD solution was found to exhibit a long-term homogeneous phase without any noticeable precipitation at room temperature for more than half a year.

The optical properties of NGQDs were investigated in their aqueous solutions. The monodispersed NGQDs emitted blue under a UV light at 365 nm, as shown in Figure S3. The fluorescence (FL) quantum yield (QY) of NGQDs was determined to be 6.42%, as measured by the absolute QY measurement method, which is comparable to that of NGQDs prepared by other methods [12, 14].

The UV-visible (UV-vis) absorption of NGQDs as a function of solution concentration is shown in Figure 5A. Apparently, there are three absorption peaks located at approximately 211 nm (5.88 eV), 268 nm (4.63 eV), and 310 nm (4.00 eV) corresponding to the electron transitions from π to π^* of C=C, C=N, and C=O [14, 29], respectively. It can be observed that the three absorption peaks decrease in the order of Abs@211>Abs@268>Abs@310 at a certain concentration and decrease with an increasing dilution fold. Figure 5B shows that the absorbance of the three peaks is proportional to the reciprocal of dilution time (1/dilution time). The slope of the three peaks also decrease in the order of Abs@211>Abs@268>Abs@310.

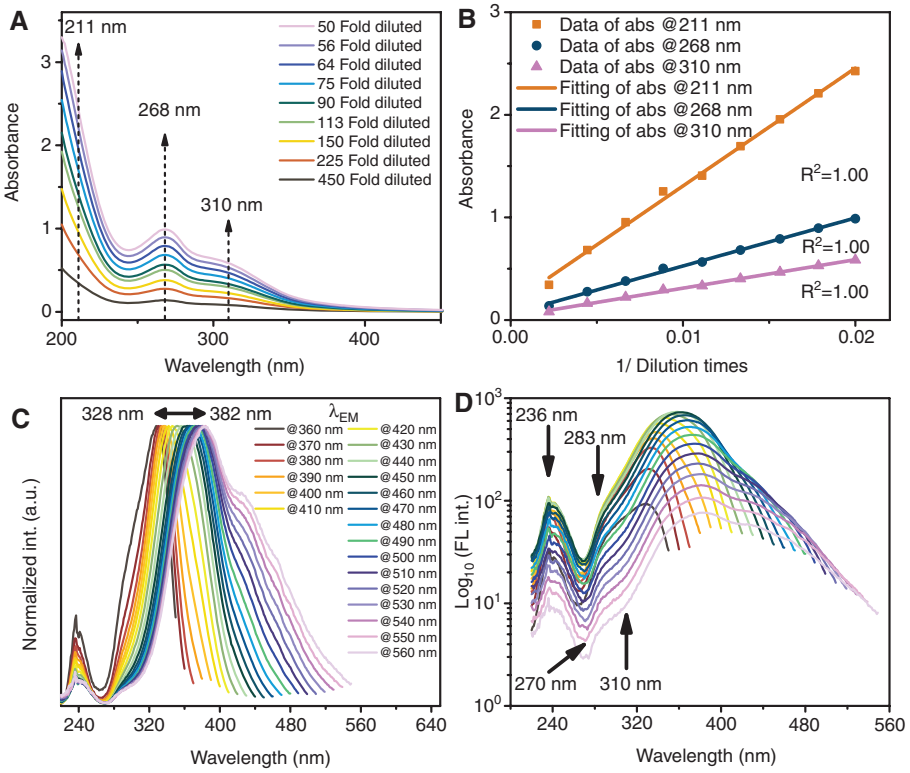

Figure 5: (A) UV-vis absorption spectra of NGQDs with different dilution folds. (B) Linear dependence of the absorbance at 211, 268, and 310 nm on 1/dilution times. (C) Normalized FLE spectra of NGQDs measured by monitoring the λ_{EM} ranging from 360 to 560 nm. (D) $\log_{10}$ (FL intensity) versus wavelength of NGQDs. Both (C) and (D) are derived from Figure S4.

The larger the absorbance is, the larger is the intrinsic density of states (DOS) of NGQDs.

The normalized FL excitation (FLE) spectra (Figure 5C) of NGQDs were derived from Figure S4, which is measured by monitoring the emission wavelength (λ_{EM}) ranging from 360 to 560 nm. Apparently, the λ_{EM}-dependent FLE peaks are limited to the range between 328 nm (3.78 eV) and 382 nm (3.25 eV), suggesting that the highest O-related excited state (O π^*, which will be mentioned later) that can emit FL is about 3.78 eV. Oppositely, the other peak located at approximately 236 nm (5.25 eV) is independent of λ_{EM}, as shown in Figure 5C and D. Another independent peak centered at approximately 283 nm (4.38 eV) is observed from the $\log_{10}$ (FL int.) plotted against wavelengths as shown in Figure 5D. These two FLE peaks correspond well to that of UV-vis absorption peaks at 211 and 268 nm. The red shift of peaks from absorption spectra to FLE spectra can be observed in previous reports of GQDs [34], S-GQDs [35], and Cl-GQDs [36], suggesting that the FLE peak corresponds to the ground vibrational state (GVS) and the peak of UV-vis absorption corresponds to the highest vibrational state (HVS) in the same excited state: GVS of C π^* is 5.25 eV, GVS of N π^* 4.38 eV, HVS of C π^* 5.88 eV, and HVS of N π^* 4.63 eV. When NGQDs absorb high-energy photons, electron transition from C π to C π^* may be caused, and then the internal conversion (C $\pi^* \rightarrow$ N $\pi^* \rightarrow$ O π^*) results in FL emission (O $\pi^* \rightarrow$ C π). The valley located at approximately 270 nm is caused by the energy gap between GVS of C π^* and HVS of N π^* and that at approximately 310 nm is caused by the energy gap between GVS of N π^* and HVS of O π^*.

The FL emission spectra of NGQDs are shown in Figure 6A. The color of the curve represents the fluorescent color of NGQDs under excitation, respectively. As shown in Figure 6A, with increasing excitation wavelength (λ_{EX}), the color of FL changes from purple to blue, cyan, and green. The FL spectra show the strongest peak at approximately 430 nm (2.82 eV), excited by λ_{EX} of 360 nm (3.44 eV). Correspondingly, a λ_{EM} of 430 nm generates the strongest FLE peak at approximately 360 nm in Figure S4, which suggests that this kind of O-related surface state has the largest density. When NGQDs are excited at wavelengths from 290 to 460 nm, the FL peak shifts from 415 nm (2.99 eV) to 511 nm (2.43 eV; Figure 6B). As shown in Figure 6C, the linear relationship between the energy of FL emission

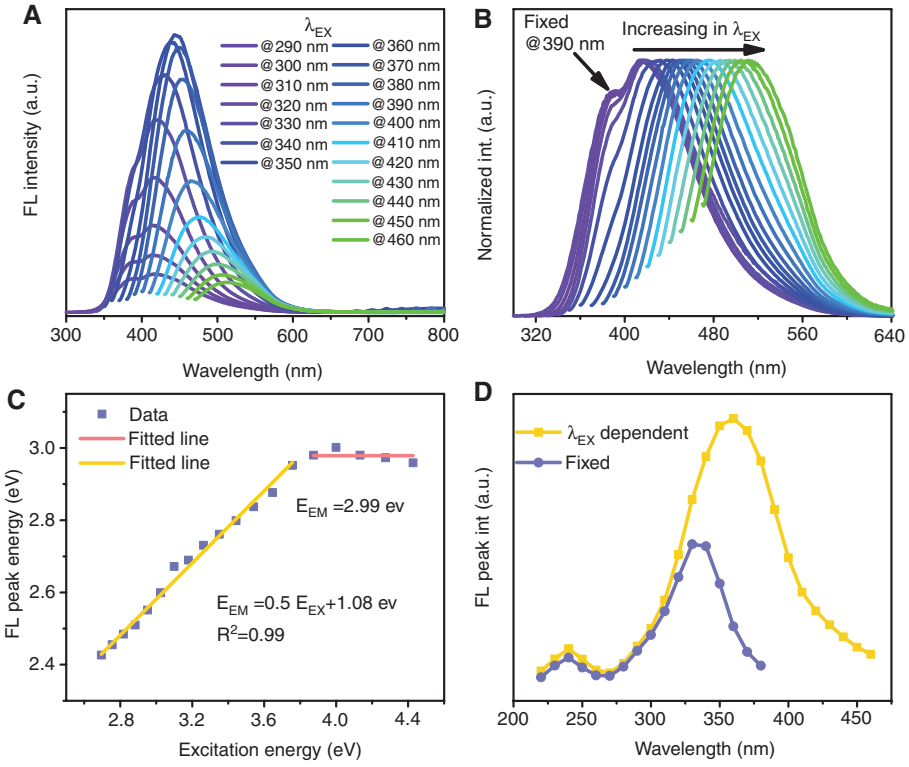

Figure 6: (A) FL emission spectra of NGQDs excited by various wavelengths ranging from 290 to 460 nm. (B) Normalized FL emission spectra of NGQDs derived from part (A). (C) Linear dependence of the FL emission peak energy on excitation energy. (D) Relationship between the intensity of two FL emission peaks (λ_{EX} dependent and fixed) and various excitation wavelengths.

peak (E_{EM}) and excitation energy (E_{EX}) can be described by the following equation:

$$E_{EM}=0.5E_{EX}+1.08 \text{ eV} \quad (1)$$

where E_{EX} is <3.77 eV (330 nm). The λ_{EX}-dependent emission may be brought about by O-related surface states (O π^*) induced by the functional groups (C-OH, C=O, C-O-C) [34]. When E_{EX} is more than 3.77 eV, E_{EM} tends to be a constant of 2.99 eV, which suggests that the highest fluorescent energy emitted by O π^* is about 2.99 eV.

Interestingly, it can also be observed that a new peak located at 390 nm (3.18 eV) is produced when E_{EX} is more than 3.77 eV in Figure 6B, confirming a higher excited state that can emit FL. The presence of this peak may result from the introduction of N into the GQDs, as this peak has not been observed for N-free GQDs [34] and its energy is lower than 4.10 eV from C π^* to C π in NGQDs [14]. Reasonably, it can be deduced that this FL emission is produced by electron recombination from N π^* to C π. Figure 6D shows the relationship between the intensity of two FL emission peaks (λ_{EX} dependent and fixed at 390 nm) on various λ_{EX} ranging from 220 to 460 nm. It can be observed that both have a peak at 240 nm and a valley at 270 nm (see Figure S5 for detail). The internal conversion from C π^* to N π^* results in FL emission (N $\pi^*\rightarrow$C π) and C π^* to O π^* results in FL emission (O $\pi^*\rightarrow$C π), further confirming the conclusion from PLE spectra.

Based on the above optical properties of NGQDs, the detailed Jablonski diagram representing the energy level structure of NGQDs can be derived, which has not been reported yet. As shown in Figure 7, the diagram illustrates the electronic states of NGQDs and the transitions between them. Four electronic states arranged vertically by energy are shown. The lowest electronic state represents the ground state of NGQDs, which is labeled as C π (C-related energy state, HOMO). At room temperature, NGQDs in a solution are in this state. The upper electronic states represent three excited states: O π^* (O-related energy state, LUMO), N π^* (N-related energy state, LUMO+1), and C π^* (C-related energy state, LUMO+2). The GVS of each electronic state is indicated with thick lines, and the numerous vibrational levels associated with each electronic state are indicated with thinner lines. When NGQDs are illuminated by light with specific wavelength, absorption transitions (straight violet and red arrows) can occur from C π to various vibrational levels in the excited vibrational states. Squiggly yellow arrows represent nonradiative transition,

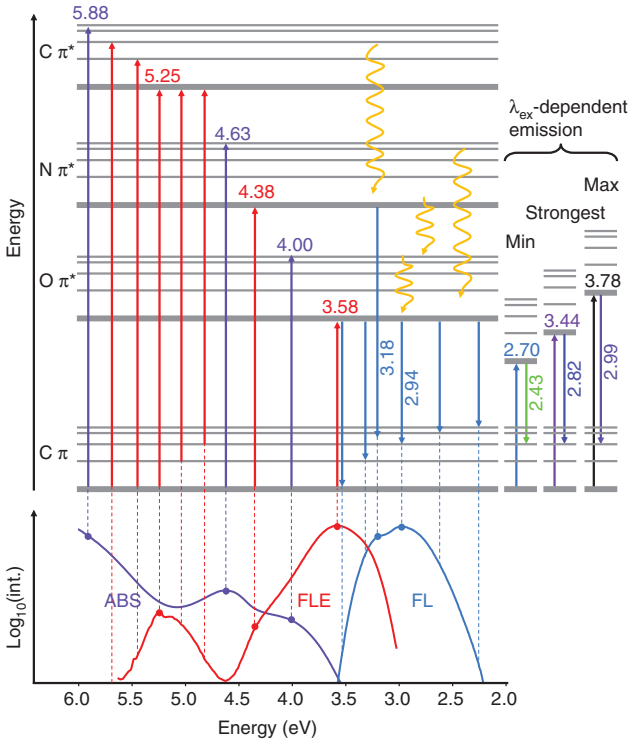

Figure 7: Jablonskidiagram (top panel) representing the energy level structure of NGQDs and the spectra (bottom panel) associated with it.

including internal conversion and vibrational relaxation process, and straight blue arrows represent FL emission. Below the diagram, the $\log_{10}$ (intensity) versus energy of UV-vis absorption, PLE@λ_{EM} of 420 nm and PL@λ_{EX} of 320 nm, are shown. The FLE peak corresponds to the GVS and the peak of UV-vis absorption corresponds to the HVS in the same excited state: C $\pi \rightarrow$C π^* (5.25–5.88 eV) and C $\pi \rightarrow$N π^* (4.38–4.63 eV). NGQDs have different kinds of O-related surface states corresponding to a relatively wide distribution of different energy levels to generate a broad UV-vis absorption band and λ_{EX}-dependent emission (right portion of diagram). The FL emission energy of O π^* is from 2.43 to 2.99 eV, and the GVS energy level is from 2.70 eV [calculated from Eq. (1)] to 3.78 eV. The strongest FL emission energy is 2.82 eV excited by excitation of 3.44 eV. It is noted that nitrogen doping introduces a new kind of excited electronic state that can emit FL at 3.18 eV. More detailed molecular orbital energy levels [37] of NGQDs should be further investigated.

3 Conclusions

We have presented an ultrafast ammonia-driven microwave-assisted synthesis of water-soluble NGQDs using glucose and ammonia solution at room temperature and atmospheric pressure. This low-cost, one-step approach is environment friendly and suitable for large-scale production. NGQDs have high crystalline quality. A new FL emission at 390 nm is observed, which might originate from the incorporation of nitrogen into the GQDs. A peak red-shift is observed by comparing FLE spectra to UV-vis absorption spectra. The detailed Jablonski diagram representing the energy level structure of NGQDs is derived: C π^* (5.25–5.88 eV), N π^* (4.38–4.63 eV), GVS of O π^* (2.70–3.78 eV), and the FL emission energy of O π^* is from 2.43 to 2.99 eV. NGQDs are promising for applications in photoelectronics and fluorescent probing.

4 Experimental

4.1 Materials

Ammonia solution (28%), quinine sulfate, and D-glucose were purchased from Aladdin (Shanghai, China). All reagents were of analytical grade and were used without further purification. The model of microwave oven is Midea EG925BYI-NAO (Guangdong, China).

4.2 Synthesis of NGQDs

First, 10 g glucose was dissolved into polypropylene container with 100 ml deionized (DI) water, and 5 ml ammonia solution was added into the solution. Then, the container (without lid) was put into a commercial microwave oven at 900 W for 1 min. After that, the solution changed from transparent to pale yellow as a result of formation of NGQDs. Subsequently, the solution was stirred vigorously at 40°C for 1 h to remove any residual ammonia. Finally, the solution was further dialyzed against DI water using a dialysis membrane with molecular weight cutoff (MWCO) of 1000 Da for characterizations.

4.3 Characterizations

TEM and HRTEM images were performed by an FEI Tecnai F20 electron microscopy operating at 200 keV. AFM images were taken using a Seiko SPA 300 AFM. The crystalline structure of the obtained samples was characterized by XRD (Rigaku D/MAX-rA diffractometer) using Cu Kα radiation. XPS was taken on an AXIS-Ultra instrument from Kratos using monochromatic Al Kα radiation operating at

150 W. The nitrogen doping content is calculated by the following equation:

$$N/C=(A_{N1s}/S_{N1s})/(A_{C1s}/S_{C1s}) \quad (2)$$

where A_{N1s} and A_{C1s} are the area of N 1s and C 1s peaks and S_{N1s} and S_{C1s} are the corresponding sensitive factors. The UV-vis absorption was measured with a Shimadzu UV-2550 spectrophotometer using 1.00 cm quartz cells. FL measurement was carried out on a Shimadzu RF-5301 PC spectrofluorophotometer with a 150 W xenon lamp as a light source using 1.00 cm quartz cells. FTIR spectra were recorded on a Shimadzu FTIR-8400S spectrophotometer using KBr pellets.

4.4 Calculation of FL QY

The FL QY of NGQDs was calculated by comparing the integrated FL intensity (excited at 360 nm) and the absorbance values at the excitation wavelength of 360 nm of NGQDs with QY standard. Quinine sulfate in 0.1 M H_2SO_4 was chosen as the standard, which has a fixed and known QY value of 54% [38]. The QY of NGQDs was calculated according to the following equation:

$$\Phi_X=\Phi_{ST}\left(\frac{Grad_X}{Grad_{ST}}\right)\left(\frac{\eta_X^2}{\eta_{ST}^2}\right) \quad (3)$$

where subscripts ST and X denote standard and test, respectively, Φ is the QY, Grad is the gradient from the plot of integrated FL intensity versus absorbance (Figure S1), and η is the refractive index of the solvent. Both the refractive indexes of NGQDs and quinine sulfate solution are 1.33.

Acknowledgments: The work was financially supported by the Fundamental Research Funds for the Central Universities (Grant No. ZYGX2013Z001), the National Natural Science Foundation of China (Grant Nos. 51202022, 51372033, and 61378028), the Specialized Research Fund for the Doctoral Program of Higher Education (Grant No. 20120185120011), the National High Technology Research and Development Program of China (Grant No. 2015AA034202), the China Electronics Technology Group Corporation of Innovative Project (Grant No. 62401110311), the 111 Project (Grant No. B13042), the Sichuan Youth Science and Technology Innovation Research Team Funding (Grant No. 2011JTD0006), the International Science and Technology Cooperation Program of China (Grant No. 2012DFA51430), and the Sino-German Cooperation PPP Program of China.

References

[1] Pan D, Zhang J, Li Z, Wu M. Hydrothermal route for cutting graphene sheets into blue-luminescent graphene quantum dots. Adv Mater 2010;22:734–8.
[2] Wang X, Tian H, Mohammad MA, Li C, Wu C, Yang Y, Ren TL. A spectrally tunable all-graphene-based flexible field-effect light-emitting device. Nat Commun 2015;6:7767.
[3] Peng J, Gao W, Gupta BK, Liu Z, Romero-Aburto R, Ge L, Song L, Alemany LB, Zhan X, Gao G, Vithayathil SA, Kaipparettu BA, Marti AA, Hayashi T, Zhu JJ, Ajayan PM. Graphene quantum dots derived from carbon fibers. Nano Lett 2012;12:844–9.
[4] Li Y, Hu Y, Zhao Y, Shi G, Deng L, Hou Y, Qu L. An electrochemical avenue to green-luminescent graphene quantum dots as potential electron-acceptors for photovoltaics. Adv Mater 2011;23:776–780.
[5] Pan D, Guo L, Zhang J, Xi C, Xue Q, Huang H, Li J, Zhang Z, Yu W, Chen Z, Li Z, Wu M. Cutting sp^2 clusters in graphene sheets into colloidal graphene quantum dots with strong green fluorescence. J Mater Chem 2012;22:3314–8.
[6] Zhao H, Chang Y, Liu M, Gao S, Yu H, Quan X. A universal immunosensing strategy based on regulation of the interaction between graphene and graphene quantum dots. Chem Commun 2013;49:234–6.
[7] Bai JM, Zhang L, Liang RP, Qiu JD. Graphene quantum dots combined with europium ions as photoluminescent probes for phosphate sensing, Chem Eur J 2013;19:3822–6.
[8] Li Y, Zhao Y, Cheng H, Hu Y, Shi G, Dai L, Qu L. Nitrogen-doped graphene quantum dots with oxygen-rich functional groups. J Am Chem Soc 2012;134:15–8.
[9] Li Q, Zhang S, Dai L, Li Ls. Nitrogen-doped colloidal graphene quantum dots and their size-dependent electrocatalytic activity for the oxygen reduction reaction. J Am Chem Soc 2012;134:18932–5.
[10] Jiang D, Zhang Y, Chu H, Liu J, Wan J, Chen M. N-doped graphene quantum dots as an effective photocatalyst for the photochemical synthesis of silver deposited porous graphitic C_3N_4 nanocomposites for nonenzymatic electrochemical H_2O_2 sensing. RSC Adv 2014;4:16163–71.
[11] Yeh TF, Teng CY, Chen SJ, Teng H. Nitrogen-doped graphene oxide quantum dots as photocatalysts for overall water-splitting under visible light illumination. Adv Mater 2014;26:3297–303.
[12] Liu Q, Guo B, Rao Z, Zhang B, Gong JR. Strong two-photon-induced fluorescence from photostable, biocompatible nitrogen-doped graphene quantum dots for cellular and deep-tissue imaging. Nano Lett 2013;13:2436–41.
[13] Ju J, Chen W. Synthesis of highly fluorescent nitrogen-doped graphene quantum dots for sensitive, label-free detection of Fe (III) in aqueous media. Biosens Bioelectron 2014;58:219–25.
[14] Tang L, Ji R, Li X, Bai G, Liu CP, Hao J, Lin J, Jiang H, Teng KS, Yang Z, Lau SP. Deep ultraviolet to near-infrared emission and photoresponse in layered n-doped graphene quantum dots. ACS Nano 2014;8:6312–20.
[15] Hu C, Liu Y, Yang Y, Cui J, Huang Z, Wang Y, Yang L, Wang H, Xiao Y, Rong J. One-step preparation of nitrogen-doped graphene quantum dots from oxidized debris of graphene oxide. J Mater Chem B 2013;1:39–42.

[16] Sun J, Yang S, Wang Z, Shen H, Xu T, Sun L, Li H, Chen W, Jiang X, Ding G, Kang Z, Xie X, Jiang M. Ultra-high quantum yield of graphene quantum dots: aromatic-nitrogen doping and photoluminescence mechanism. Part Part Syst Char 2015;32:434–40.
[17] Dai Y, Long H, Wang X, Wang Y, Gu Q, Jiang W, Wang Y, Li C, Zeng TH, Sun Y, Zeng J. Versatile graphene quantum dots with tunable nitrogen doping. Part Part Syst Char 2014;31:597–604.
[18] Li M, Wu W, Ren W, Cheng HM, Tang N, Zhong W, Du Y. Synthesis and upconversion luminescence of n-doped graphene quantum dots. Appl Phys Lett 2012;101:103107.
[19] Dey S, Govindaraj A, Biswas K, Rao CNR. Luminescence properties of boron and nitrogen doped graphene quantum dots prepared from arc-discharge-generated doped graphene samples. Chem Phys Lett 2014;595–596:203–8.
[20] Xu H, Zhou S, Xiao L, Wang H, Li S, Yuan Q. Fabrication of a nitrogen-doped graphene quantum dot from MOF-derived porous carbon and its application for highly selective fluorescence detection of Fe^{3+}. J Mater Chem C 2015;3:291–7.
[21] Li L, Li L, Wang C, Liu K, Zhu R, Qiang H, Lin Y. Synthesis of nitrogen-doped and amino acid-functionalized graphene quantum dots from glycine, and their application to the fluorometric determination of ferric ion. Microchim Acta 2015;182:763–70.
[22] Tam TV, Trung NB, Kim HR, Chung JS, Choi WM. One-pot synthesis of n-doped graphene quantum dots as a fluorescent sensing platform for Fe^{3+} ions detection. Sensor Actuat B-Chem 2014;202:568–73.
[23] Cai F, Liu X, Liu S, Liu H, Huang Y. A simple one-pot synthesis of highly fluorescent nitrogen-doped graphene quantum dots for the detection of Cr(VI) in aqueous media. RSC Adv 2014;4:52016–22.
[24] Wu ZL, Gao MX, Wang TT, Wan XY, Zheng LL, Huang CZ. A general quantitative ph sensor developed with dicyandiamide n-doped high quantum yield graphene quantum dots. Nanoscale 2014;6:3868–74.
[25] Ju J, Zhang R, He S, Chen W. Nitrogen-doped graphene quantum dots-based fluorescent probe for the sensitive turn-on detection of glutathione and its cellular imaging. RSC Adv 2014;4:52583–9.
[26] Lin L, Rong M, Lu S, Song X, Zhong Y, Yan J, Wang Y, Chen X. A facile synthesis of highly luminescent nitrogen-doped graphene quantum dots for the detection of 2,4,6-trinitrophenol in aqueous solution. Nanoscale 2015;7:1872–8.
[27] Shi B, Zhang L, Lan C, Zhao J, Su Y, Zhao S. One-pot green synthesis of oxygen-rich nitrogen-doped graphene quantum dots and their potential application in ph-sensitive photoluminescence and detection of mercury(II) ions. Talanta 2015;142:131–9.
[28] Sun X, Li Y. Colloidal carbon spheres and their core/shell structures with noble-metal nanoparticles. Angew Chem Int Ed 2004;43:597–601.
[29] Tang L, Ji R, Li X, Teng KS, Lau SP. Energy-level structure of nitrogen-doped graphene quantum dots. J Mater Chem C 2013;1:4908–15.
[30] Zhu H, Wang X, Li Y, Wang Z, Yang F, Yang X. Microwave synthesis of fluorescent carbon nanoparticles with electrochemiluminescence properties. Chem Commun 2009;5118–20.
[31] Wang X, Qu K, Xu B, Ren J, Qu X. Microwave assisted one-step green synthesis of cell-permeable multicolor photoluminescent carbon dots without surface passivation reagents. J Mater Chem 2011;21:2445–50.
[32] Palaniselvam T, Valappil MO, Illathvalappil R, Kurungot S. Nanoporous graphene by quantum dots removal from graphene and its conversion to a potential oxygen reduction electrocatalyst via nitrogen doping. Energ Environ Sci 2014;7:1059–67.
[33] Wang Z, Li P, Chen Y, Liu J, Tian H, Zhou J, Zhang W, Li Y. Synthesis of nitrogen-doped graphene by chemical vapour deposition using melamine as the sole solid source of carbon and nitrogen. J Mater Chem C 2014;2:7396–401.
[34] Tang L, Ji R, Cao X, Lin J, Jiang H, Li X, Teng KS, Luk CM, Zeng S, Hao J, Lau SP. Deep ultraviolet photoluminescence of water-soluble self-passivated graphene quantum dots. ACS Nano 2012;6:5102–10.
[35] Li X, Lau SP, Tang L, Ji R, Yang P. Sulphur doping: a facile approach to tune the electronic structure and optical properties of graphene quantum dots. Nanoscale 2014;6:5323–8.
[36] Li X, Lau SP, Tang L, Ji R, Yang P. Multicolour light emission from chlorine-doped graphene quantum dots. J Mater Chem C 2013;1:7308–13.
[37] Sarkar S, Sudolská M, Dubecký M, Reckmeier CJ, Rogach AL, Zbořil R, Otyepka M. Graphitic nitrogen doping in carbon dots causes red-shifted absorption. J Phys Chem C 2016;120:1303–8.
[38] Melhuish WH. Quantum efficiencies of fluorescence of organic substances: effect of solvent and concentration of the fluorescent solute. J Phys Chem 1961;65:229–35.

Supplemental Material: The online version of this article (DOI: 10.1515/nanoph-2016-0102) offers supplementary material, available to authorized users.